

RESEARCH ARTICLE

10.1002/2016JA022557

Key Points:

- Ionospheric instability does not cause CPCP saturation
- Magnetosheath parameters that regulate reconnection most relevant to CPCP saturation
- Models that regulate reconnection using magnetosheath parameters are most relevant

Correspondence to:

C. R. Clauer,
rclauer@vt.edu

Citation:

Clauer, C. R., Z. Xu, M. Maimaiti, J. M. Ruohoneimi, W. Scales, M. D. Hartinger, M. J. Nicolls, S. Kaeppler, F. D. Wilder, and R. E. Lopez (2016), Investigation of a rare event where the polar ionospheric reverse convection potential does not saturate during a period of extreme northward IMF solar wind driving, *J. Geophys. Res. Space Physics*, 121, doi:10.1002/2016JA022557.

Received 19 FEB 2016

Accepted 4 JUN 2016

Accepted article online 10 JUN 2016

Investigation of a rare event where the polar ionospheric reverse convection potential does not saturate during a period of extreme northward IMF solar wind driving

C. Robert Clauer¹, Zhonghua Xu¹, M. Maimaiti¹, J. Michael Ruohoneimi¹, Wayne Scales¹, Michael D. Hartinger¹, Michael J. Nicolls², Stephen Kaeppler², Frederick D. Wilder³, and Ramon E. Lopez⁴

¹Bradley Department of Electrical and Computer Engineering, Virginia Polytechnic Institute and State University, Blacksburg, Virginia, USA, ²Center for Geospace Studies, SRII, Menlo Park, California, USA, ³Laboratory for Atmospheric and Space Physics, University of Colorado Boulder, Boulder, Colorado, USA, ⁴Department of Physics, University of Texas at Arlington, Arlington, Texas, USA

Abstract A variety of statistical studies have shown that the ionospheric polar potential produced by solar wind-magnetosphere-ionosphere coupling is linear for weak to moderate solar wind driving but becomes nonlinear during periods of very strong driving. It has been shown that this applies to the two-cell convection potential that develops during southward interplanetary magnetic field (IMF) and also to the reverse convection cells that develop during northward IMF. This has been described as polar potential saturation, and it appears to begin when the driving solar wind electric field becomes greater than 3 mV/m. Utilizing measurements from the Resolute Incoherent Scatter Radar (RISR-N), we examine ionospheric data near local noon within the reverse convection cells that developed during a period of very strong northward interplanetary magnetic field (IMF) on 12 September 2014. During this period we measure the electric field within the throat of the reverse convection cells to be near 150 mV/m at a time when the IMF is nearly 28 nT northward. This is far in excess of the 30–40 mV/m expected for polar potential saturation of the reverse convection cells. In fact, the development of the electric field responds linearly to the IMF B_z component throughout this period of extreme driving. The conditions in the solar wind show the solar wind velocity near 600 km/s, number density near 20 ions/cm³, and the Alfvén velocity about 75 km/s giving an Alfvén Mach number of 8. A search of several years of solar wind data shows that these values occur together 0.035% of the time. These conditions imply a high plasma β in the magnetosheath. We believe that condition of high β along with high mass density and a strong merging electric field in the magnetosheath are the significant parameters that produce the linear driving of the ionospheric electric field during this unusual period of extreme solar wind conditions. A discussion of current theories to account for cross-polar cap potential saturation is given with the conclusion that theories that utilize magnetosheath parameters as they affect the reconnection rate appear to be the most relevant to the cross-polar cap potential saturation solution.

1. Introduction

A key measure of the interaction that couples energy and momentum from the solar wind to the magnetosphere-ionosphere system is the electric cross-polar cap potential (CPCP). Early investigations have shown a linear relationship between the solar wind driving of the magnetosphere, measured by southward interplanetary magnetic field (IMF) and the CPCP [Reiff *et al.*, 1981; Reiff and Luhmann, 1986]. Later investigations that examined a larger range of magnetospheric driving associated with magnetospheric storms and superstorms found that at extreme levels of southward IMF, the relationship becomes nonlinear. This phenomenon has often been described as polar potential “saturation”; however, it has never been shown that the potential develops to some asymptotic level. In fact, it appears to continuously increase but at a lesser rate. The nonlinear development of the cross-polar cap potential has been shown by several investigations using global arrays of observations. Some investigations used the assimilative mapping of ionospheric electrodynamic inversion of a global distribution of magnetometer data to show that the potential begins to “saturate”

as the driving of the magnetosphere by the solar wind increases to very strong levels [Russell *et al.*, 2001; Liemohn *et al.*, 2002]. A similar nonlinear development of the ionospheric CPCP was demonstrated using DMSP ion drift measurements during periods of magnetic storms [Hairston *et al.*, 2003; Ober *et al.*, 2003; Hairston *et al.*, 2005]. Using Super Dual Auroral Radar Network (SuperDARN) global ionospheric radar measurements to determine the polar potential distribution, Shepherd *et al.* [2002] reported a statistical investigation of polar cap potentials that also showed the potential to develop linearly at low-to-moderate IMF southward values and to then become nonlinear at larger southward IMF values. Wilder *et al.* [2010, 2011] reproduce Shepherd's result using a different methodology to analyze the SuperDARN measurements. Further, global numerical simulations of the solar wind interaction with the magnetosphere have also shown the phenomena of polar potential saturation [Siscoe *et al.*, 2002a, 2002b; Raeder *et al.*, 2001; Merkin *et al.*, 2003; Lopez *et al.*, 2009, 2010].

When the IMF is northward, reconnection occurs poleward of the cusp on lobe field lines [Dungey, 1963; Watanabe *et al.*, 2005; Dorelli *et al.*, 2007]. The resulting convection pattern consists of four cells. Two cells exhibit antisunward flow at higher latitudes and return flow at lower latitudes due to viscous coupling. The other two are reverse convection cells at high latitudes on the dayside that exist as a result of lobe reconnection [Crooker, 1992]. The reverse convection cells are thought to be driven by high-latitude field-aligned currents termed NBZ by Iijima *et al.* [1984]. NBZ refers to the fact that the field-aligned currents form when the IMF B_z component is directed northward. Wilder *et al.* [2008] demonstrated that the electric potential across the NBZ ionospheric convection cells, Φ_{RC} , also exhibits nonlinear saturation. The average fitted potential across the reverse convection cells saturated at approximately 20 kV. Sundberg *et al.* [2009] also demonstrated saturation of the reverse convection potential using drift meter data from the DMSP satellites. Interestingly, Wilder *et al.* [2010] report that the values of the saturation electric field for both southward and northward IMFs are nearly the same at approximately 20 mV/m. Investigation of the saturation of the reverse convection potential during northward IMF using global MHD simulation methods has also been reported by Bhattarai *et al.* [2012].

Present theories concerning the cause of the observed limit to the polar electric potential focus on limiting the coupling between the solar wind and the magnetosphere during periods of strong solar wind driving. The Siscoe-Hill model, for example, involves a feedback mechanism from the ionosphere to the magnetosphere [Hill *et al.*, 1976; Siscoe *et al.*, 2002a]. Under strong driving, the region 1 currents, which close at the ionosphere and the outer magnetosphere, limit the magnetic field at the subsolar magnetopause, which limits the reconnection rate and, as a consequence, causes CPCP to saturate. According to this model, the solar wind ram pressure also plays a role. Siscoe *et al.* [2002b] postulated that under saturation, the region 1 current replaces the Chapman-Ferraro currents and provides the $\mathbf{J} \times \mathbf{B}$ force necessary to stand off the solar wind.

Another hypothesis for explaining polar cap potential saturation was given by Kivelson and Ridley [2008], sometimes referred to as the "Alfvén wing" model. According to this model, there is a mismatch in conductance between the source electric field (in the solar wind) and the ionospheric electric field. This mismatch causes a portion of the electric field imposed on the ionosphere to be reflected, which leads to the saturation of the cross-polar cap potential, Φ_{pc} . The conductivity at the source is controlled mainly by the Alfvénic speed in the solar wind ($\Sigma_A = [\mu_0 V_A]^{-1}$), while, in the ionosphere, the controlling conductivity is the Pedersen conductivity. The portion of the driving electric field that is transmitted to the polar cap is represented by the Kivelson-Ridley coupling function E_{KR}

$$E_{KR} = \frac{2E_{sw}}{1 + \Sigma_p/\Sigma_A}$$

where E_{sw} is the portion of the interplanetary electric field (IEF) observed at Earth that is imposed on the magnetosphere via reconnection and Σ_p is the height-integrated Pedersen conductivity in the ionosphere. Typically, as the IMF increases in magnitude, the Alfvén speed increases and the Alfvénic conductance decreases. The decrease in Alfvénic conductance causes the nonlinear response of the polar cap potential and electric field.

Recently, Lopez *et al.* [2010] proposed that the nonlinear saturation effect can be explained by considering the magnetosheath flow that actually reaches the merging line. Typically, only a fraction of the solar wind flow incident on the magnetosphere actually reaches the merging line since most of the flow is deflected around the magnetosphere by forces on the flow in the magnetosheath. Under normal solar wind Mach number [≈ 8 , e.g., Ridley, 2007] conditions the pressure gradient is the dominant force on the magnetosheath flow. Since this force does not depend on the magnitude of the IMF, a larger IMF will not change the amount

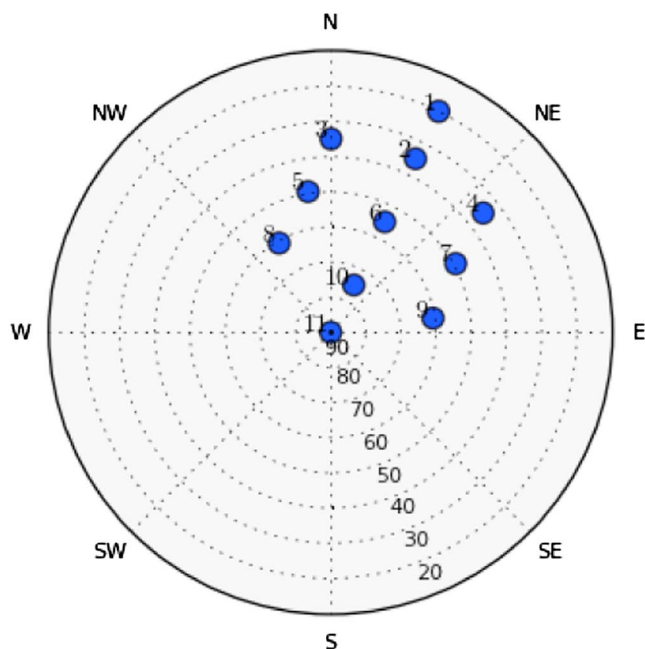


Figure 1. Azimuth and elevation locations for the 11 radar beam positions used in the RISR-N measurements on 12 September 2014. Geographic directions are indicated around the diagram. Concentric circles indicate elevation angle for the radar beam. Position 11 is nominally up the local magnetic field line.

of flow reaching the merging line. Thus, the same flow delivers more magnetic flux to the merging line, producing a correspondingly larger potential. For solar wind with fast mode Mach number of about 3 or less, the magnetosheath plasma has $\beta < 1$. This means that the $\mathbf{J} \times \mathbf{B}$ force will become the dominant force on the magnetosheath flow. Since the $\mathbf{J} \times \mathbf{B}$ force on the magnetosheath plasma does depends on the IMF magnitude, a larger IMF produces a larger $\mathbf{J} \times \mathbf{B}$ force, producing a larger diversion of the magnetosheath flow away from the merging line. So even though the amount of magnetic flux in solar wind flow is greater, the amount of flow that reaches the merging line is less, and this limits the reconnection potential.

In an attempt to test these theories for ionospheric electric potential saturation *Wilder et al.* [2011] conducted a statistical investigation into the relation of solar wind properties on the saturation of the cross-polar cap potential (CPCP) during periods of strongly southward IMF. They found that the nonlinear trend in the relationship between the interplanetary coupling electric field and the CPCP is best fitted with a square root function and that the CPCP does not exhibit asymptotic behavior. Correlations of the CPCP with various interplanetary parameters showed a weak but statistically significant correlation with solar wind Alfvénic Mach number and no significant correlation with solar wind dynamic pressure. These results do not provide strong support for any of the existing hypotheses.

On the other hand, it is clear that the conductivity of the ionosphere plays an important role in the electro-dynamics of the solar wind-magnetosphere-ionosphere system. What is not clear is how local ionospheric electro-dynamics plays into the saturation phenomenon. *Winglee et al.* [2002], for example, demonstrate that increased O⁺ outflow can have a limiting effect on the polar cap potential. The heavier ions have a “mass loading” effect and limit the momentum of plasma convection in the magnetosphere. Up to now there has been little consideration of the role that the ionosphere may play in the CPCP saturation phenomenon. It is, therefore, worth investigating to see whether or not there is an ionospheric mechanism which limits either the current or electric field.

As noted above, *Wilder et al.* [2010] examined the electric potential saturation for the reverse convection cells that form during northward IMF and found that while the potential was smaller than the potential that developed across the polar cap during southward IMF potential saturation, the electric fields saturate at about the same value for both cases, between 20 and 40 mV/m depending upon season. This observation suggests that perhaps the cause of saturation lies wholly or partially within the ionosphere. For example, within the auroral electrojets, the Farley-Buneman instability may develop to produce an anomalous resistivity that effectively

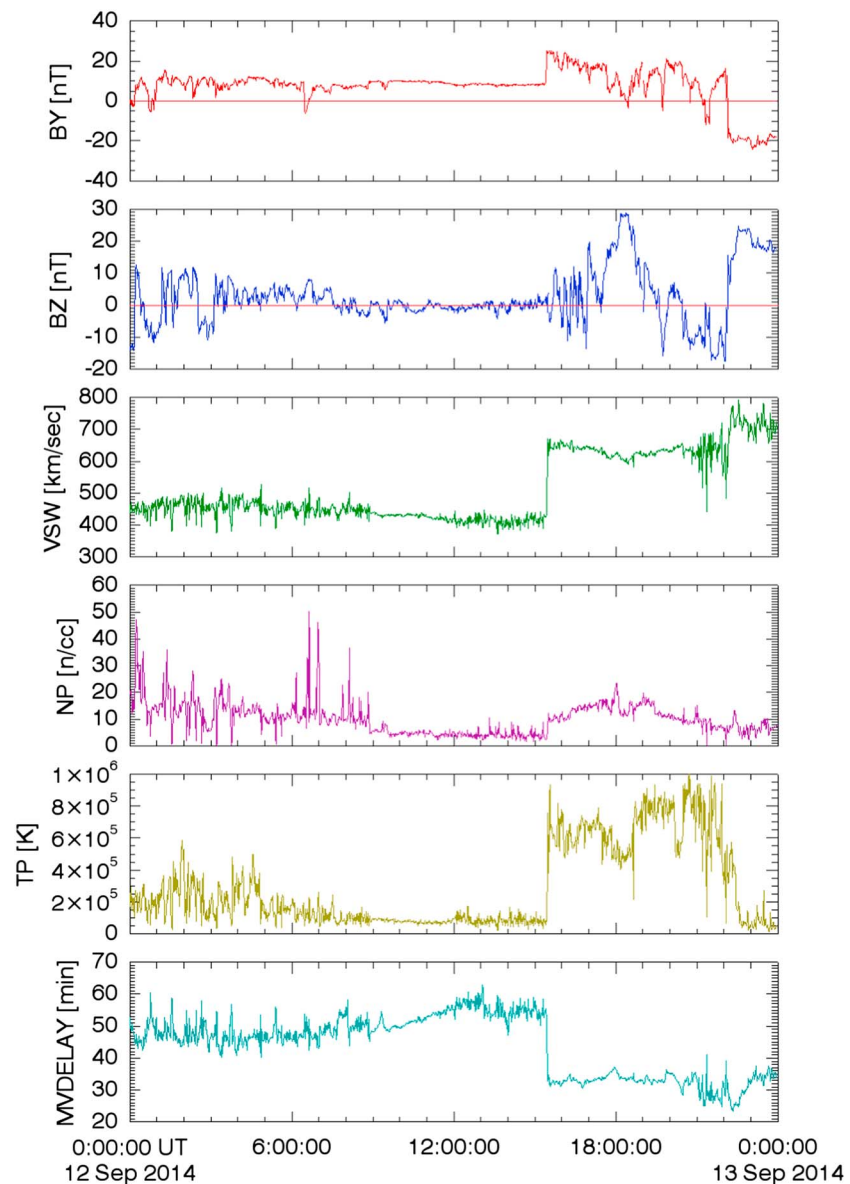


Figure 2. ACE satellite real-time measurements of solar wind properties on 12 September 2014. (first and second panels) Interplanetary magnetic field Y and Z components in GSM coordinates. (third panel) Solar wind velocity toward the Earth. (fourth and fifth panels) Solar wind proton number density and temperature, respectively. (sixth panel) The estimated time delay between the satellite and the Earth's magnetopause.

limits the local E region electric field [St.-Maurice, 1987]. The extent to which this saturation of the E region electric field may manifest itself in the F region and upward into the magnetosphere is an open question. Perhaps during periods of strong energy coupling between the solar wind, magnetosphere, and ionosphere, the Farley-Buneman or some other plasma instabilities can develop in the polar cap to limit the convection.

This investigation began to investigate the ionosphere in the vicinity of the throat of the reverse convection cells during periods of extreme northward IMF solar wind driving using the northward facing Resolute Incoherent Scatter Radar (RISR-N). The hypothesis to be examined is that extreme driving may produce ionospheric plasma instabilities at some threshold level of driving, and this will limit the further development of the electric field. In this way the ionosphere is not just a passive medium but an active element in the coupled system that provides feedback that affects the coupling dynamics. Below we report the results from our first set of experiments that produced a fortuitous set of measurements during unusual and extremely rare set of solar wind conditions that produced extreme driving of the reverse convection cells. The conditions in

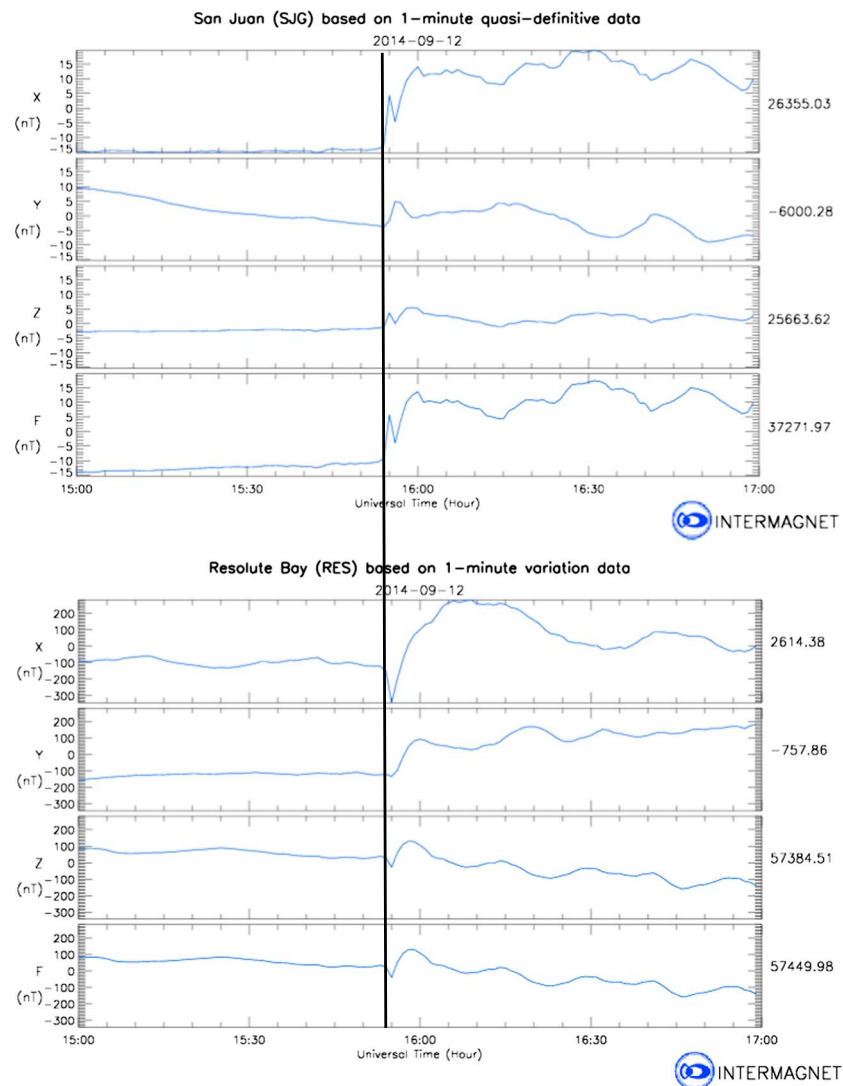


Figure 3. Standard magnetograms from (top) San Juan Puerto Rico and (bottom) Resolute Bay. The sudden compression of the dayside field by the solar wind shock is clearly identified by the sudden increase in the *X* (northward) component at San Juan at 1554 UT. Data are provided by Intermagnet.

the solar wind produced an ionospheric reverse convection electric field that does not saturate and reaches values near 150 mV/m. This event, therefore, shows that there are more parameters to the saturation problem than just the level of the driving electric field. Thus, this event can provide new insights to the various theories that attempt to account for polar potential saturation. Through an examination of this rare event in which saturation is not observed it is possible to develop our understanding of the processes that are required to produce saturation of the polar convection electric field. While these observations are for the case of northward IMF, we believe that the conclusions that we can obtain may be applied to the case for southward IMF as well.

2. Measurements on 12 September 2014

The primary measurements examined here are produced by the Resolute Bay incoherent scatter radar (north directed face) RISR-N located at a geographic latitude of 74.72955° north and longitude -94.90576° east. Magnetic local noon at the radar is at about 19 UT. The radar is able to make measurements poleward of the magnetospheric cusp near local noon and is thus ideally positioned to measure the region of the throat between the reverse convection cells that form during periods of northward IMF. The instrument uses a phased array antenna to make measurements at 11 positions poleward along and to either side of the magnetic

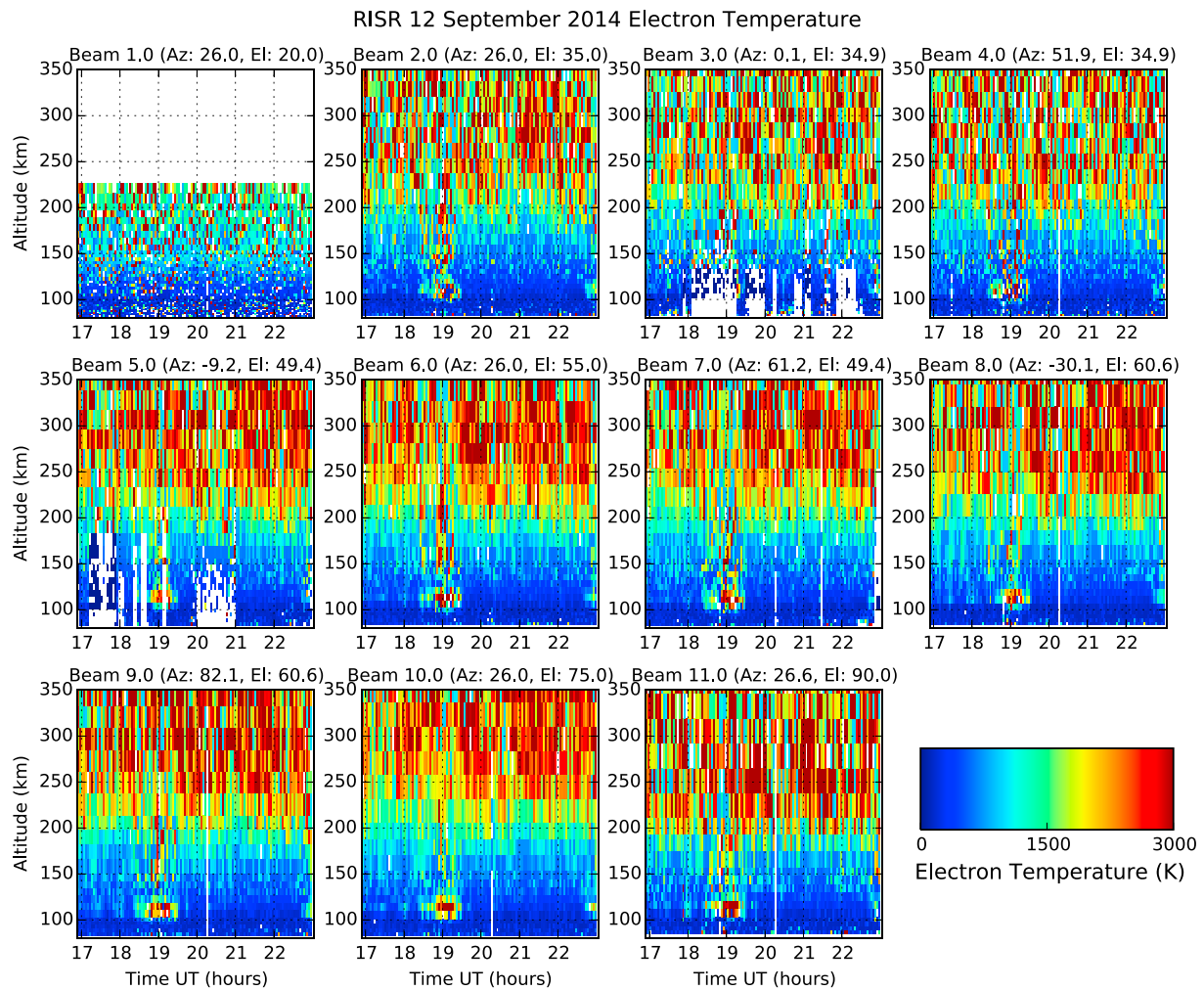


Figure 4. Electron temperature in degrees kelvin measured from 17 UT to 23 UT on 12 September 2014 as a function of time and altitude. Heating in the E region (100 km altitude) can be seen in most beams from 18:30 UT to 19:30 UT during the period of strong convection and strong northward IMF.

meridian including one position up the local magnetic field line. More information regarding the radar, its operation, and capabilities are given in *Bahcivan et al.* [2010]. Figure 1 shows the spatial coverage in azimuth and elevation for the 11 beams. The radar was operated using a combined long-pulse, alternating-code experiment on 12 September 2014, the day of interest in this paper. The long pulse gives good resolution in the F region but limited resolution in the E region. The alternating code provides measurements at E region altitudes.

We utilize only GSM coordinates for solar wind parameters throughout this paper. Figure 2 shows the solar wind parameters measured by the ACE satellite upstream from the Earth on 12 September 2014. An interplanetary shock is observed to cross ACE at about 15:30 UT. This is indicated by a sudden increase in velocity from roughly 450 km/s to 600 km/s together with a sharp increase in plasma density and temperature. The shock is the result of an interplanetary coronal mass ejection. Following the shock is a sheath (strong oscillations in B_z) followed by a magnetic cloud (strong field slowly rotating). The B_z component in the cloud shows a period of northward IMF at about 17:20 UT and strongly northward field (about 28 nT) for 20 min just after 18 UT. This period of extremely strong northward IMF coincides with the time that RISR-N is near local noon and is able to measure ionospheric parameters in the throat of the reverse convection cells that develop during periods of northward IMF. The time that the interplanetary shock impacts the magnetosphere can be determined very exactly by looking at a dayside low-latitude ground magnetometer station. Figure 3 shows the magnetic measurements obtained at San Juan (top) and Resolute Bay (bottom) from 15 UT to 17 UT on 12 September 2014. The vertical line at 1554 UT shows the results of the impact of the solar wind shock with

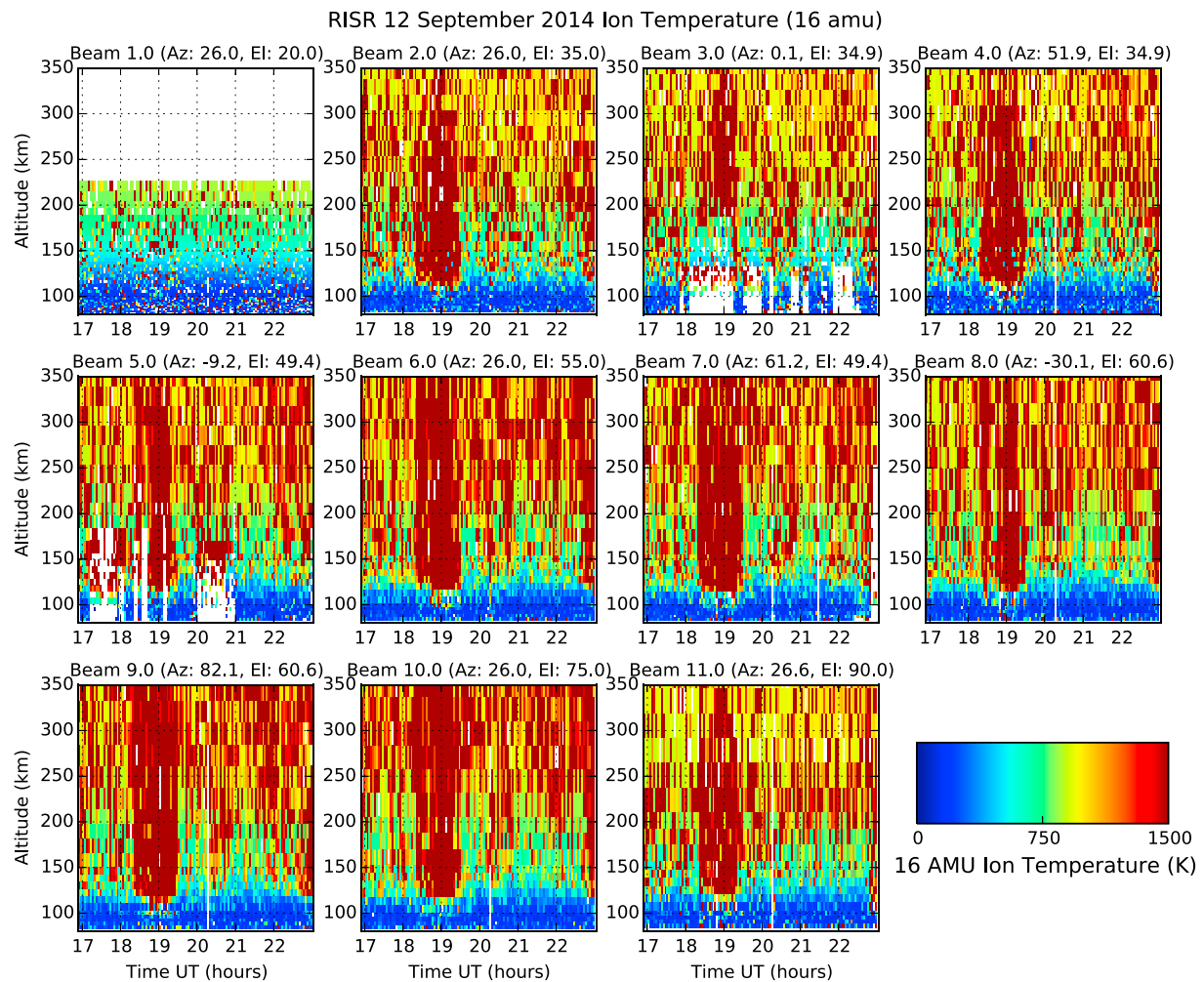


Figure 5. Ion temperature in degrees kelvin measured from 17 UT to 23 UT on 12 September 2014 as a function of time and altitude. Heating in the *E* region (100 km altitude) and above in the *F* region can be seen in most beams from 18:30 to 19:30 UT during the period of strong convection and strong northward IMF.

the magnetopause as seen at the surface of the Earth. The period of northward IMF is observed at the ACE satellite to follow the shock front by about 2.5 h. Thus, we might expect to observe the effects of the northward IMF beginning between 18:00 and 18:30 UT.

Figure 4 shows the ionospheric electron temperature as a function of time (horizontal axis) and altitude (vertical axis) at each of the 11 dwell locations shown in Figure 1. In the majority of the panels there is an enhancement in the *E* region electron temperatures measured by the alternating code at about 100 km during the period of strong northward IMF interaction with the magnetosphere (approximately 18:30–19:30 UT). Figure 5 shows a similar set of plots for the ion temperatures. Most of these plots show ion heating in both the *E* and *F* regions during the period of strong northward IMF interaction with the magnetosphere.

Next we look at the development of the ionospheric electric field in the throat of the reverse convection cells measured by RISR-N. The ionospheric line-of-sight plasma velocity is measured by the doppler shift in the radar return pulse. Using locations on either side of the magnetic meridian, it is possible to derive the horizontal plasma velocity under the assumption of spatial and temporal uniformity of the plasma flow [Heinselmann and Nicolls, 2008]. Knowing that the flow is produced by $\mathbf{E} \times \mathbf{B}$ drift and knowing the magnetic field, it is possible to derive the ionospheric electric field that is driving the plasma flow. In Figure 6 we show measurements of the IMF at the ACE satellite together with the ionospheric electric field measured at 84° magnetic latitude in the center of the RISR-N field of view. There is no time shift of the satellite data. From the top of the plot we

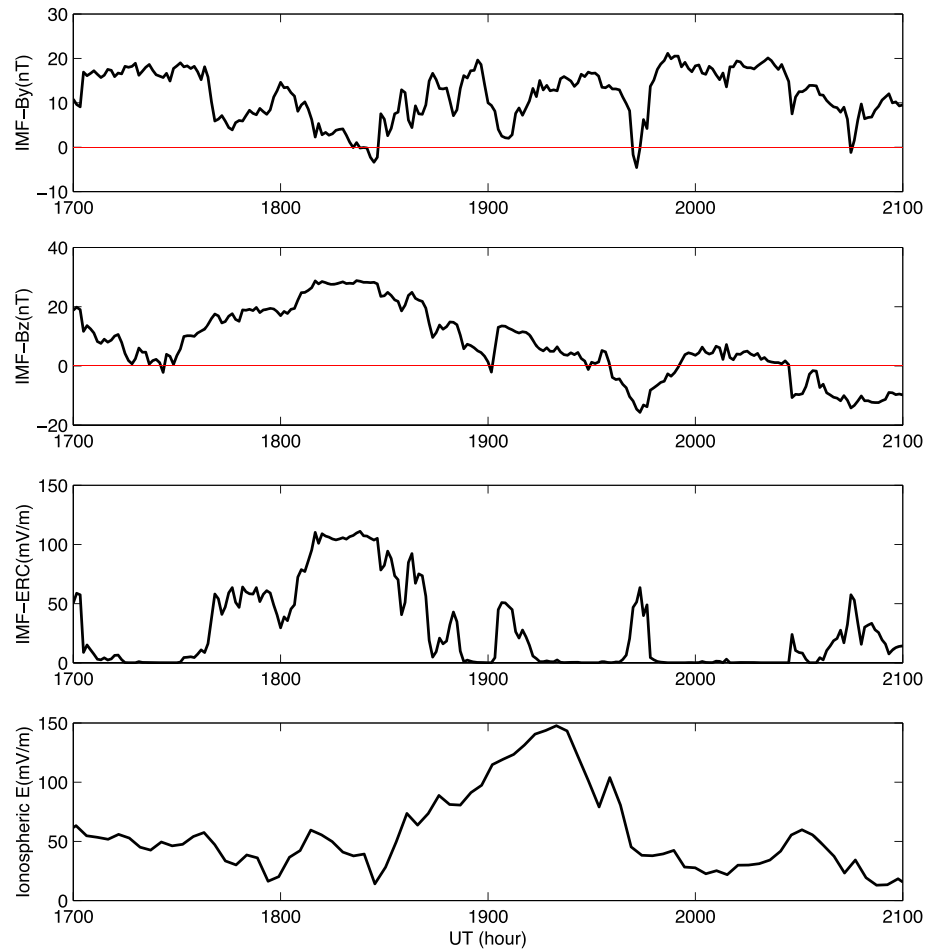


Figure 6. ACE real-time solar wind data. (first and second panels) IMF B_y and B_z components, respectively. (third and fourth panels) The IMF coupling electric field function for northward IMF and reverse convection cells E_{RC} and the ionospheric horizontal electric field measured at 84° magnetic latitude by RISR-N.

show the IMF B_y and B_z components. Figure 6 (third panel) shows the computed value of solar wind coupling function E_{RC} for northward IMF and reverse convection, defined by *Wilder et al.* [2008] as

$$E_{RC} = -V_x B_T \cos^4 \theta$$

where $B_T = \sqrt{B_y^2 + B_z^2}$ is the transverse magnetic field and $\theta = \arccos\left(\frac{B_z}{\sqrt{B_y^2 + B_z^2}}\right)$ is the IMF clock angle in the Y-Z plane. The value of E_{RC} is a geometric coupling function for northward IMF similar to the coupling function for southward IMF proposed by *Sonnerup* [1974] and later utilized by *Kan and Lee* [1979] defined as

$$E_{KL} = V_x B_T \sin^2 \frac{\theta}{2}$$

Figure 6 (fourth panel) shows the ionospheric electric field derived from the RISR-N measurements at 84° . Looking at Figure 6 (third and fourth panels), the strong IMF northward produces a strong E_{RC} beginning just after 18 UT that is followed about 1 h later with very strong ionospheric electric fields reaching nearly 150 mV/m after 19 UT. *Wilder et al.* [2008] reported that the ionospheric electric field in the reverse convection potentials saturates at between 20 mV/m and 40 mV/m. So measuring 150 mV/m during this event is extraordinary. We notice also that the ionospheric electric field between 17 and 18 UT is often around 50 mV/m which is also perhaps significant. This occurs during moderately northward IMF and also very strong IMF B_y . The strong B_y moves the reconnection site toward the dusk flank in the Northern Hemisphere and produces a strong “banana-cell” convection on the morning side of the polar ionosphere. In this analysis, however,

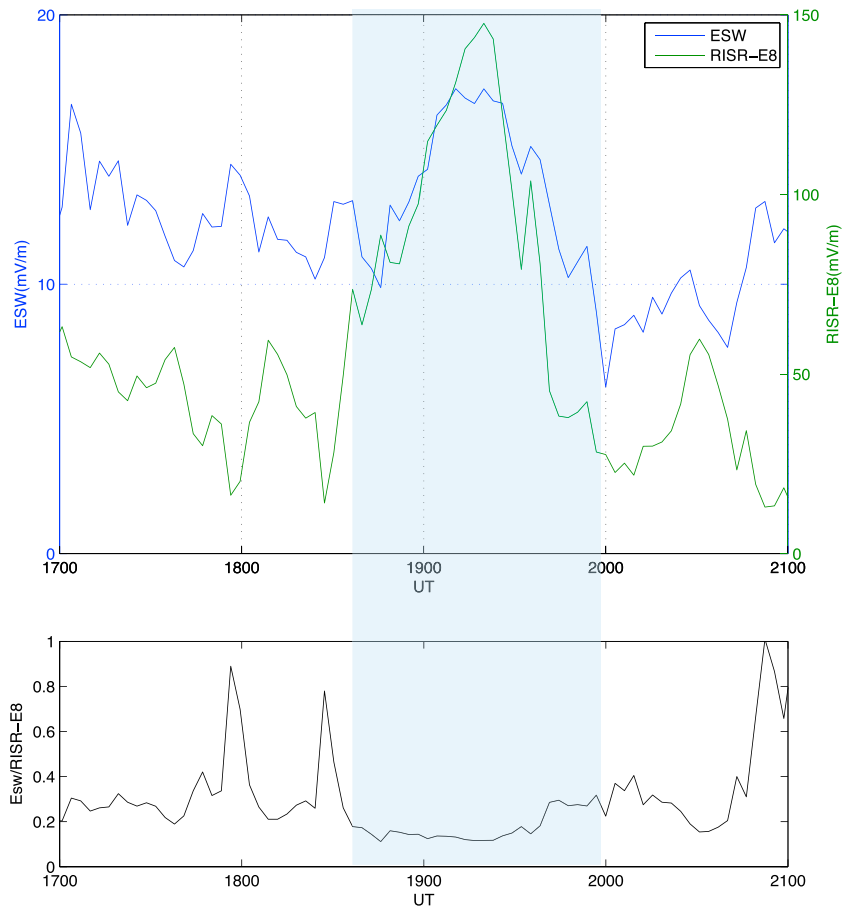


Figure 7. The horizontal axis shows time on 12 September 2014. (top) The blue trace shows the solar wind electric field component in the YZ plane (left ordinate) and the green trace shows the ionospheric horizontal electric field determined by the ion velocity measured by RISR-N (right ordinate). The ACE real-time solar wind data have been shifted by 55 min to align best with the ionospheric measurements, as determined by eye. The shaded portion of the plot is the period of interest when the IMF is primarily northward, and RISR-N is measuring the ion flow in the throat of the reverse convection cells. (bottom) The ratio between the plotted ionospheric electric field and the solar wind electric field. Note that for the period of interest the ratio is constant.

we are concentrating our attention to the period of strong northward IMF and weaker IMF B_y between 18:30 and 19:30 UT.

To examine the development of the electric field in the ionospheric throat between the two reverse convection cells, we have compared the average ionospheric electric field computed from the ion velocity measured over the central beams 10, 6, and 2 to the solar wind electric field in the Y-Z plane ($V_x \sqrt{B_y^2 + B_z^2}$). This is shown in Figure 7. The green trace shows the ionospheric electric field determined from the ionospheric velocity measured near local magnetic noon with scale on the right vertical axis. The blue trace shows the driving solar wind electric field component with a 55 min delay to align with the ionospheric velocity measurements as determined by eye. The solar wind electric field scale is shown on the left vertical axis. Universal time is shown on the horizontal axis from 17 UT to 21 UT. At about 18:30 UT the IMF B_z component turns northward and the ionospheric electric field increases together with the positive B_z showing an almost linear relationship through the entire interval from 18:30 to 19:35 UT. Figure 7 (bottom) shows the ratio of the electric field traces plotted at the top of the figure. The shaded portion indicates the period of interest where the IMF is primarily northward and RISR-N is measuring the ionospheric flows in the throat of the reverse convection cells. For that period of interest, the ratio is constant and the ionospheric electric field is roughly 10 times the driving electric field E_y in the solar wind.

The shock was observed at ACE at 15:20 UT, and B_z turned northward at 17:25 reaching greater than 20 nT at 18 UT. Thus, the duration of the sheath is about 2 h and 5 min. The shock is observed at the dayside ground

station at 15:54 indicating a lag of 34 min from ACE. Thus, we would expect the northward turning of the IMF to arrive at the magnetopause at about 18 UT and to become greater than 20 nT at the magnetopause at about 18:35 UT using the 34–35 min propagation time. Since we shift by 55 min, there is a 20 min difference that could correspond to the reconfiguration time required for the ionospheric convection to fully develop [Clauer and Friis-Christensen, 1988].

3. Discussion

The observations here show that the relationship between the level of solar wind driving measured by some function of IMF and solar wind velocity, and the polar ionospheric electric field is more complex than the original polar potential saturation papers would suggest. Other factors must play a role as to whether the electric field imposed on the ionosphere from the coupling of the solar wind with the magnetosphere through merging develops linearly or nonlinearly. In the case presented here, the electric field between the reverse convection cells develops linearly as the solar wind driving function increases to extremely high levels, far beyond the level where the relationship is thought to become nonlinear.

Our initial goal was to determine if ionospheric instabilities such as the Farley-Buneman instability might develop and limit the electric field development in the ionosphere through some feedback mechanism. Indeed, we see electric fields develop in the ionosphere in excess of the threshold usually thought to trigger the Farley-Buneman instability and we measure *E* region heating consistent with the development of plasma instabilities. However, since there is no saturation of the electric field in this event, it seems clear that this mechanism is not capable of producing the saturation phenomenon and we therefore dismiss this idea.

As discussed by Siscoe *et al.* [2002a] the model of solar wind-magnetosphere-ionosphere coupling presented by Hill *et al.* [1976] and Hill [1984] explains the saturation phenomenon as a nonlinear process that results from a feedback in which the magnetic field generated by the region 1 currents becomes comparable to and opposes the Earth's dipole field at the magnetopause where reconnection occurs. The weakening of the field that is reconnecting ultimately limits how fast reconnection can occur. The result is that at low levels of solar wind driving, reconnection at the magnetopause taps a fraction of the solar wind potential across the magnetopause and this is coupled to the ionosphere via equipotential magnetic field lines to produce an ionospheric potential that is roughly linearly related to the solar wind driving potential. For high levels of solar wind driving, the ionosphere begins to control the potential since the region 1 currents are regulated by the ionospheric conductance as well as the driving voltage. While this formulation is for the case of southward IMF, it probably has relevance also for northward reconnection as well. We discuss this because it brings consideration of other potentially relevant parameters, such as ionospheric Pedersen conductivity, solar wind Mach number, and solar wind Alfvén velocity.

Siscoe *et al.* [2002a] express the reconnection potential at the magnetopause as

$$\Phi_M \approx \chi L_{r0} R_E E_{sw} P_{sw} D^{1/3} F(\theta)$$

where L_{r0} is the effective length of the reconnection line in units of R_E and E_{sw} is the intensity of the motional electric field in the solar wind $V_{sw} B_{sw}$ where sw indicates solar wind quantities. V is the velocity, and B is the magnetic field; P is the ram pressure ($\rho_{sw} V_{sw}^2$), and ρ is the mass density. D is the dipole strength normalized to the present value, and $F(\theta)$ represents the IMF clock angle (in the *Y-Z* plane) dependence geometry for reconnection. The coefficient χ quantifies the effects of magnetosheath compression and reconnection efficiency: $\chi = 4f_r (2\kappa \rho_{sw} / \rho_{sh})^{1/2}$ where f_r is a reconnection efficiency factor given by the ratio of reconnection velocity (or inflow velocity) to Alfvén velocity, sh indicates values in the magnetosheath, and κ is the ratio of the stagnation pressure to the solar wind ram pressure, which depends upon solar wind Mach number. For low Mach numbers κ is near unity and for high Mach numbers it is of order 0.88. The value of L_{r0} is usually expressed as a constant, around 6 or 7 R_E . In the magnetosheath force balance model of Lopez *et al.* [2010], however, this length is given by the divergence of the flow in the magnetosheath around the magnetosphere, which depends on the amount of force per unit volume on the plasma as well as the dynamic pressure of the flow. Nevertheless, in either case, for northward IMF, the geoeffective length L_{r0} is probably closer to 1 R_E , reflecting the less efficient merging geometry for northward IMF.

For the case under consideration, the solar wind velocity is near 600 km/s and the Alfvén velocity is about 75 km/s so the Alfvén Mach number is 8. While an Alfvén Mach number of 8 is not unusual for typical solar

wind values of $V \approx 400$ km/s, $B \approx 5$ nT, and a few ions/cm³, it is extremely rare and high for a solar wind velocity of 600 km/s, a 30 nT magnetic field, and 20 ions/cm³. In the 5 year interval (1 January 2010 to 1 January 2015) there were 904 min of data in the OMNI data set in which the IMF magnitude was greater than 20 nT and the Alfvénic Mach number was between 5 and 8. That is 0.035% of the total data, so these solar wind conditions are rare. Indeed, most of the data that meet these criteria are included in the event under consideration here. So in this instance, 8 is a high Mach number and high Mach number tends to correlate with high plasma β in the magnetosheath [Mullan and Smith, 2006]. Low Alfvénic Mach number is theoretically required to limit reconnection and therefore leads to CPCP saturation. Our observations support this theoretical understanding because the inferred lack of low plasma β in the magnetosheath is associated with a linear relation between the solar and driving electric field and the ionospheric reverse convection electric field with no indication of nonlinear saturation occurring. Thus, the observations here seem consistent with the Lopez *et al.* [2010] magnetosheath force balance model. The large number density during this event decreases the Alfvén velocity below what would be expected from the large magnitude of B under typical solar wind conditions. Thus, Σ_A would be increased in the Alfvén wing model and this could also account for the linear response observed during this event by that model.

The polar cap potential is given in Siscoe *et al.* [2002a] by the expression

$$\Phi_{pc} = \Phi_M \Phi_S / (\Phi_M + \Phi_S) = \frac{\Phi_M}{1 + \frac{\Phi_M}{\Phi_S}}$$

where Φ_S is the saturation potential. The strength of the region 1 current is related to the ionospheric Ohm's law and the Pedersen conductivity, and the saturation potential is related to the saturation current in the Siscoe-Hill model. According to Borovsky and Denton [2006], saturation of Φ_{pc} occurs when the second term in the denominator exceeds approximately 2. This occurs when $V_A \Sigma_p / 806 > 2$, where V_A is the Alfvén velocity in the upstream solar wind (in units of km/s) and Σ_p is the height-integrated Pedersen conductivity of the dayside ionosphere (in units of mho). We can approximate $\Sigma_p = 0.77 \sqrt{F_{10.7}}$, where $F_{10.7}$ is the radio emission flux from the Sun at 10.7 cm that is used as a proxy for the solar EUV emission that ionizes the Earth's upper atmosphere. Using this, Borovsky and Denton [2006] transform the inequality into

$$Q = \frac{V_A \sqrt{F_{10.7}}}{1050.2} > 2$$

where Q is called the saturation parameter. For the conditions during the event on 12 September 2014, we compute $V_A = 75.38$ km/s and find $F_{10.7} = 130$. Using these values we get $Q = 0.81$. Thus, according to this formulation, even though the driving is extreme, saturation should not occur, consistent with our observations. In this formulation, the ionospheric conductivity and the solar wind magnetic field and mass density are the parameters that determine if the CPCP will develop linearly or nonlinearly with respect to the solar wind reconnection electric field.

Since we have RISR measurements, however, it is possible to determine directly the Pedersen and Hall conductivities from the incoherent scatter return spectrum. Figure 8 shows the derived Pedersen (top) and Hall (middle) conductivities. Figure 8 (bottom) shows the height-integrated Hall and Pedersen conductance. At its maximum, the height-integrated Hall conductance is just under 8 mhos. Typical values for these latitudes near local noon are around 4 mhos [Hardy *et al.*, 1987]. During the interval from 18:00 to 19:30 UT the height-integrated conductance varies from nearly 8 mhos to values mostly around 4 or 5 mhos. At 18 UT, the height-integrated Pedersen conductivity is 4 and varies between 2 and 6 during the interval to 19:30 UT. These observations do not rule out high Pedersen conductance as an important parameter to enable the saturation process since the conductance values vary between somewhat high to typical.

In the formulation of the Lopez *et al.* [2010] magnetosheath force balance model, current generated at the bow shock closes through the magnetosheath to the magnetopause and couples with Birkeland currents. Under moderate solar wind driving conditions, the gradient in the plasma pressure controls the magnetosheath flow. However, at large IMF magnitudes (southward) the bow shock current system and currents in the magnetosheath can become significant to the point where the $\mathbf{J} \times \mathbf{B}$ force becomes dominant. As the driving increases, the $\mathbf{J} \times \mathbf{B}$ force diverts more flow away from the merging line thus decreasing the effective length of the reconnection line. This is responsible for limiting the development of the CPCP at times of strong

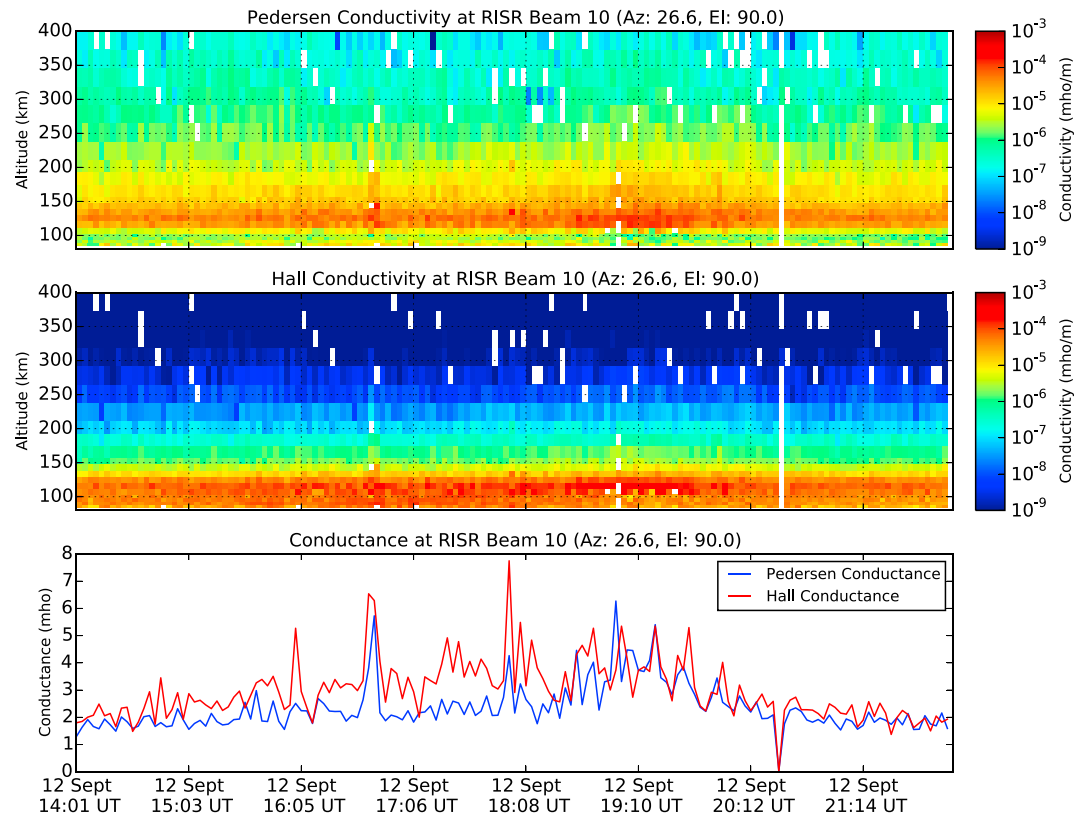


Figure 8. (top) Pedersen and (middle) Hall conductivities measured by RISR-N along beam 10 (nearly up the field line) (see Figure 1) as a function of time. (bottom) high-integrated Hall (red) and Pedersen (blue) conductance computed from the measurements shown in the top and middle panels.

driving. Thus, in this model, the transition from a magnetosheath flow dominated by plasma pressure to one dominated by magnetic pressure determines if the CPCP development is linear or becomes nonlinear. Thus, the operative parameter is the plasma β in the magnetosheath. We note that the ionosphere also plays a role since the region 1 currents are important to determine the shape of the magnetosphere flaring angle. Increased conductivity could enhance the region 1 currents. The enhanced region 1 currents at dawn and dusk would reduce the northward geomagnetic field in the subsolar region and enhance the northward field throughout the nightside. This would increase the flaring angle with the consequence of increasing the pressure in the magnetosheath.

4. Conclusions

As discussed in the introduction, we initiated the RISR measurements to see if we could identify ionospheric plasma instabilities that might develop during strong driving and provide a feedback that plays a role in limiting the development of the ionospheric electric field. We were hopeful when we saw the E region heating during the period of very large northward IMF. However, seeing that the ionospheric electric field continued to develop linearly with the strength of the positive IMF B_z component, we are inclined to believe that this is not an important mechanism, or is, at best, of secondary importance.

The extremely rare conditions in the solar wind that produce extreme driving while also producing a high β magnetosheath seem to be the best explanation for the lack of CPCP electric field saturation. This indicates that the conditions in the magnetosheath that contribute to enhancing or limiting reconnection are most important in the CPCP saturation explanation. This provides strong support for the Lopez model but does not necessarily eliminate the Siscoe-Hill or Alfvén wing mechanisms. Nevertheless, it does demonstrate that models that utilize magnetosheath parameters as they affect the reconnection rate appear to be the most relevant to the CPCP saturation solution.

Acknowledgments

Support for this research at Virginia Tech is provided by NSF grants AGS-1216373, AGS1049403, and AGS-13341918. F.D.W. is supported by NSF GEM grant AGS-1303649. The Resolute Incoherent Scatter Radar (RISR-N) is operated by SRI International on behalf of the U.S. National Science Foundation under NSF Cooperative Agreement AGS-1133009. R.E.L. acknowledges support from NASA grant NNX15AJ03G. We also wish to acknowledge the use of the NASA/GFSC Space Physics Data Facility's OMNIWeb and CDASWeb service and the OMNI database and Intermagnet. The RISR-N data are available in the Madrigal Archival Database (madrigal.haystack.mit.edu) or directly from SRIL in Menlo Park, CA.

References

- Bahcivan, H., R. Tsunoda, M. Nicolls, and C. Heinselman (2010), Initial ionospheric observations made by the new Resolute incoherent scatter radar and comparison to solar wind IMF, *Geophys. Res. Lett.*, *37*, L15103, doi:10.1029/2010GL043632.
- Bhattarai, S. K., R. E. Lopez, R. Bruntz, J. G. Lyon, and M. Wiltberger (2012), Simulation of the polar cap potential during periods with northward interplanetary magnetic field, *J. Geophys. Res.*, *117*, A04219, doi:10.1029/2011JA017143.
- Borovsky, J. E., and M. H. Denton (2006), Differences between CME-driven storms and CIR-driven storms, *J. Geophys. Res.*, *111*, A07S08, doi:10.1029/2005JA011447.
- Clauer, C. R., and E. Friis-Christensen (1988), High-latitude dayside electric fields and currents during strong northward IMF: Observations and model simulation, *J. Geophys. Res.*, *93*, 2749–2757.
- Crooker, N. U. (1992), Reverse convection, *J. Geophys. Res.*, *97*, 19,363–19,372, doi:10.1029/92JA01532.
- Dorelli, J., A. Bhattacharjee, and J. Raeder (2007), Separator reconnection at Earth's dayside magnetopause under northward interplanetary magnetic field conditions, *J. Geophys. Res.*, *112*, A02202, doi:10.1029/2006JA011877.
- Dungey, J. (1963), The structure of the exosphere or adventures in velocity space, in *Geophysics, The Earth's Environment*, edited by C. DeWitt, J. Hieblot, and A. Lebeau, pp. 505, Gordon and Breach, New York.
- Hairston, M., T. Hill, and R. Heelis (2003), Observed saturation of the ionospheric polar cap during the 31 March 2001 storm, *Geophys. Res. Lett.*, *30*(6), 1325, doi:10.1029/2002GL015894.
- Hairston, M. R., K. A. Drake, and R. Skoug (2005), Saturation of the ionospheric polar cap potential during the October–November 2003 superstorms, *J. Geophys. Res.*, *110*, A09S26, doi:10.1029/2004JA010864.
- Hardy, D., M. Gussenhoven, R. Raistrick, and W. McNeil (1987), Statistical and functional representation of the pattern of auroral energy flux, number flux, and conductivity, *J. Geophys. Res.*, *92*(A11), 12,275–12,294, doi:10.1029/JA092iA11p12275.
- Heinselman, C. J., and M. J. Nicolls (2008), A Bayesian approach to electric field and E-region neutral wind estimation with the Poker Flat Advanced Modular Incoherent Scatter Radar, *Radio Sci.*, *43*, RS5013, doi:10.1029/2007RS003805.
- Hill, T., A. J. Dessler, and R. A. Wolf (1976), Mercury and Mars: The role of ionospheric conductivity in the acceleration of magnetospheric particles, *Geophys. Res. Lett.*, *3*, 429–432.
- Hill, T. W. (1984), Magnetic coupling between the solar wind and magnetosphere: Regulated by ionospheric conductance?, *Eos Trans. AGU*, *65*(45), 1047.
- Iijima, T., T. A. Potemra, L. J. Zanetti, and P. F. Bythrow (1984), Large-scale Birkeland currents in the dayside polar region during strongly northward IMF: A new Birkeland current system, *J. Geophys. Res.*, *89*(A9), 7441–7452, doi:10.1029/JA089iA09p07441.
- Kan, J. R., and L. C. Lee (1979), Energy coupling function and solar wind magnetosphere dynamo, *Geophys. Res. Lett.*, *6*(7), 577–580, doi:10.1029/GL006i007p00577.
- Kivelson, M. G., and A. J. Ridley (2008), Saturation of the polar cap potential: Inference from Alfvén wing arguments, *J. Geophys. Res.*, *113*, A05214, doi:10.1029/2007JA012302.
- Liemohn, M. W., J. U. Kozyra, M. R. Hairston, D. M. Weimer, G. Lu, A. J. Ridley, T. H. Zurbuchan, and R. M. Skoug (2002), Consequences of a saturated convection electric field on the ring current, *Geophys. Res. Lett.*, *29*(9), 62–1–62–4, doi:10.1029/2001GL014270.
- Lopez, R. E., J. G. Lyon, E. Mitchell, R. Bruntz, V. G. Merkin, S. Brogl, F. Toffoletto, and M. Wiltberger (2009), Why doesn't the ring current injection rate saturate?, *J. Geophys. Res.*, *114*, A02204, doi:10.1029/2008JA013141.
- Lopez, R. E., R. J. Bruntz, E. J. Mitchell, M. Wiltberger, and J. G. Lyon (2010), The role of magnetosheath force balance in regulating the dayside reconnection potential, *J. Geophys. Res.*, *115*, A12216, doi:10.1029/2009JA014597.
- Merkin, V. G., K. Papadopoulos, G. Milikh, A. S. Sharma, X. Shao, J. Lyon, and C. Goodrich (2003), Effects of the solar wind electric field and ionospheric conductance on the cross polar cap potential: Results of global MHD modeling, *Geophys. Res. Lett.*, *30*(23), 2180, doi:10.1029/2003GL017903.
- Mullan, D. J., and C. W. Smith (2006), Solar wind statistics at 1 AU: Alfvén speed and plasma beta, *Sol. Phys.*, *234*, 325–338, doi:10.1007/s11207-006-2-77-y.
- Ober, D. M., N. C. Maynard, and W. J. Burke (2003), Testing the Hill model of transpolar potential saturation, *J. Geophys. Res.*, *108*(A12), 1467, doi:10.1029/2003JA010154.
- Raeder, J., Y. L. Wang, T. J. Fuller-Rowell, and H. J. Singer (2001), Global simulation of space weather effects on the Bastille Day storm, *Sol. Phys.*, *204*, 323–337, doi:10.1023/A:1014228230714.
- Reiff, P., R. Spiro, and T. Hill (1981), Dependence of polar cap potential on interplanetary parameters, *J. Geophys. Res.*, *86*, 7639–7648.
- Reiff, P. H., and J. G. Luhmann (1986), Solar wind control of the polar cap voltage, in *Solar Wind-Magnetosphere Coupling*, edited by Y. Kamide and J. A. Slavin, pp. 507, Terra Scientific Publ., Tokyo, Japan.
- Ridley, A. (2007), Alfvén wings at the earth's magnetosphere under strong interplanetary magnetic field, *Ann. Geophys.*, *25*(2), 533–542.
- Russell, C. T., J. G. Luhmann, and G. Lu (2001), Nonlinear response of the polar ionosphere to large values of the interplanetary electric field, *J. Geophys. Res.*, *106*, 18,495–18,504.
- Shepherd, S. G., R. A. Greenwald, and J. M. Ruohoniemi (2002), Cross polar cap potentials measured with Super Dual Auroral Radar Network during quasi-steady solar wind and interplanetary magnetic field conditions, *J. Geophys. Res.*, *107*(A7), 1094, doi:10.1029/2001JA000152.
- Siscoe, G. L., G. M. Erickson, B. U. O. Sonnerup, N. C. Maynard, J. A. Schoendorf, K. D. Siebert, D. R. Weimer, W. W. White, and G. R. Wilson (2002a), Hill model of transpolar potential saturation: Comparisons with MHD simulations, *J. Geophys. Res.*, *107*(A6), 1075, doi:10.1029/2001JA000109.
- Siscoe, G. L., N. U. Crooker, and K. D. Siebert (2002b), Transpolar potential saturation: Roles of region 1 current system and solar wind ram pressure, *J. Geophys. Res.*, *107*(A10), 1321, doi:10.1029/2001JA009176.
- Sonnerup, B. U. O. (1974), Magnetopause reconnection rate, *J. Geophys. Res.*, *79*, 1546–1549.
- St.-Maurice, J.-P. (1987), A unified theory of anomalous resistivity and Joule heating effects in the presence of ionospheric E region irregularities, *J. Geophys. Res.*, *92*(A5), 4533–4542.
- Sundberg, K. Å. T., J. A. Cumnock, and L. G. Bloomberg (2009), Reverse convection potential: A statistical study of the general properties of lobe reconnection and saturation effects during northward IMF, *J. Geophys. Res.*, *114*, A06205, doi:10.1029/2008JA013838.
- Watanabe, M., K. Kabin, G. J. Sofko, R. Rankin, T. I. Gombosi, A. J. Ridley, and C. R. Clauer (2005), The internal reconnection for northward interplanetary magnetic field, *J. Geophys. Res.*, *110*, A06210, doi:10.1029/2004JA010832.
- Wilder, F. D., C. R. Clauer, and J. B. H. Baker (2008), Reverse convection potential saturation during northward IMF, *Geophys. Res. Lett.*, *35*, L12103, doi:10.1029/2008GL034040.

- Wilder, F. D., C. R. Clauer, and J. B. H. Baker (2010), Polar cap electric field saturation during interplanetary magnetic field B_z north and south conditions, *J. Geophys. Res.*, *115*, A10230, doi:10.1029/2010JA015487.
- Wilder, F. D., C. R. Clauer, J. B. H. Baker, E. D. Pettigrew, and M. R. Hairston (2011), The nonlinear response of the polar cap potential under southward IMF—A statistical view, *J. Geophys. Res.*, *116*(A12229), doi:10.1029/2011JA016924.
- Winglee, R., D. Chua, M. Brittnacher, G. Parks, and G. Lu (2002), Global impact of ionospheric outflows in the dynamics of the magnetosphere and cross polar cap potential, *J. Geophys. Res.*, *107*(A9), 1237, doi:10.1029/2002JA009241.